

Three dimensional high-order gas-kinetic scheme for supersonic isotropic turbulence II: coarse-grained analysis of compressible K_{sgs} budget

Guiyu Cao^a, Liang Pan^b, Kun Xu^{a,c,*}

^a*Department of Mathematics, Hong Kong University of Science and Technology, Clear Water Bay, Kowloon, Hong Kong*

^b*School of Mathematical Sciences, Beijing Normal University, Beijing, China*

^c*Shenzhen Research Institute, Hong Kong University of Science and Technology, Shenzhen, China*

Abstract

The direct numerical simulation (DNS) of compressible isotropic turbulence up to the supersonic regime $Ma_t = 1.2$ has been investigated by high-order gas-kinetic scheme (HGKS) [*Computers & Fluids*, 192, 2019]. In this study, the coarse-grained analysis of subgrid-scale (SGS) turbulent kinetic energy K_{sgs} budget is fully analyzed for constructing one-equation SGS model in the compressible large eddy simulation (LES). The DNS on a much higher turbulent Mach number up to $Ma_t = 2.0$ has been obtained by HGKS, which confirms the super robustness of HGKS. Then, the exact compressible SGS turbulent kinetic energy K_{sgs} transport equation is derived with density weighted filtering process. Based on the compressible K_{sgs} transport equation, the coarse-grained processes are implemented on three sets of unresolved grids with the Box filter. The coarse-grained analysis of compressible K_{sgs} budgets shows that all unresolved source terms are dominant terms in current system. Especially, the magnitude of SGS pressure-dilation term is in the order of SGS solenoidal dissipation term within the initial acoustic time scale. Therefore, it can be concluded that the SGS pressure-dilation term cannot be neglected as the previous work. The delicate coarse-grained analysis of SGS diffusion terms in compressible K_{sgs} equation confirms that both the fluctuation velocity triple correlation term and the pressure-velocity correlation term are dominant terms. Current coarse-grained analysis gives an indication of the order of magnitude of all SGS terms in compressible K_{sgs} budget, which provides a solid basis for compressible LES modeling in high Mach number turbulent flow.

Keywords: High-order gas-kinetic scheme, supersonic isotropic turbulence, compressible K_{sgs} transport equation, coarse-grained budget analysis

*Corresponding author

Email addresses: gcaooa@connect.ust.hk (Guiyu Cao), panliang@bnu.edu.cn (Liang Pan), makxu@ust.hk (Kun Xu)

1. Introduction

The supersonic turbulence plays a key role in a wide range of natural phenomena and engineering applications, such as interstellar turbulence, hypersonic spacecraft reentry, and nuclear fusion power reactors [1, 2]. Compared with incompressible turbulence, highly compressible turbulent flows are more complex due to nonlinear coupling of the velocity, density and pressure fields [3]. To elucidate the effects of compressibility in the compressible turbulence, the compressible isotropic turbulence is regarded as one of cornerstones [4, 5, 6]. However, for the compressible isotropic turbulence in supersonic regime ($Ma_t \geq 0.8$), the stronger random shocklets and higher spatial-temporal gradients pose greater difficulties for both theoretical analyses and numerical studies than the flow in other regime [5, 7, 8]. Currently, the study of supersonic regime is much less known and reported, and very few numerical experiments are available [9, 8, 10].

For compressible turbulence modeling, the large eddy simulation (LES) for high Mach number turbulent flows is also reported rarely. One-equation subgrid-scale (SGS) models have been extensively used in incompressible LES [11, 12, 13, 14]. Since the incorporation of history and non-local effects through transport equation related to the residual motions, the one-equation SGS models have shown better performance in the prediction of turbulent flow. Meanwhile, compared with the abundant research on compressibility correction for the turbulent kinetic energy equation in Reynolds averaged Navier-Stokes (RANS) simulation [15, 16, 17, 18, 19, 20, 21], for compressible LES, there only exists limited number of research work on compressible one-equation SGS models [22, 23, 24, 25]. With the rapid increasing of computational power, it is well known that the LES gradually becomes the workhorse for high-fidelity turbulence simulation from the smooth turbulent flow to the supersonic one [26]. However, as far as we know, the compressible LES models are less reported, where the algebraic eddy viscosity model can be hardly incorporated with the compressible effect systematically [27, 28]. In the modeling of the compressible effect, it is natural to extend the one-equation SGS model to high turbulent Mach number flow. For compressible one-equation SGS model, an important issue that has not been resolved in the earlier studies is how to distinguish the dominant terms and negligible ones. Very few coarse-grained analysis of compressible turbulence has been carried out in LES [29, 30, 31], where most of them are limited to the subsonic turbulent Mach number ($Ma_t \leq 0.8$). The priori tests using direct numerical simulation (DNS) data for the calculation of a mixing layer up to Mach number 0.6 [29, 30], and the DNS for the homogeneous isotropic turbulence up to $Ma_t = 0.52$, were filtered, and the unclosed terms in the momentum, internal energy, and total energy equations were computed [31]. It is emphasized that the unresolved dilational dissipation rate and the unresolved pressure-dilation term are important to the compressible LES. For the forced supersonic isotropic turbulence ($Ma_t \approx 1.0$), the filtered result of turbulent kinetic energy transfer on unresolved grids has been well studied [32]. While, with the orientation of constructing one-equation SGS model for a much higher turbulent Mach number flow, i.e., $Ma_t \geq 1.0$, the detailed analysis of coarse-grained turbulent kinetic energy budget K_{sgs} is much required in the modeling.

In the past decades, the gas-kinetic scheme (GKS) based on the Bhatnagar-Gross-Krook

(BGK) model [33, 34] has been developed systematically for the computations from low speed flow to hypersonic one [35, 36, 37]. With the multi-stage multi-derivative framework [38], a reliable GKS has been constructed with fourth-order and even higher-order accuracy with the implementation of the traditional second-order or third-order flux functions [39, 40, 41, 42]. In recent years, GKS has been applied in high-Reynolds number turbulent flow [43, 44]. More importantly, considering the high-order accuracy in the coupled evolution in space and time, and the super robustness of high-order gas-kinetic scheme (HGKS), the HGKS has been used in the DNS for compressible isotropic turbulence up to the supersonic regime $Ma_t = 1.2$ [8]. This study confirms that HGKS provides a valid tool for supersonic isotropic turbulence simulation, and the criterion for a correct DNS solution is determined. Following the first part [8], in order to construct one-equation SGS model for compressible LES, the coarse-grained analysis on supersonic isotropic turbulence is studied here. In this paper, the DNS on a much higher turbulent Mach number ($Ma_t = 2.0$) has been conducted, which confirms the super robustness of HGKS. Then, the exact compressible turbulent kinetic energy K_{sgs} transport equation has been derived through a density weighted filtering process. Based on the high-fidelity DNS data, coarse-graining processes are implemented in physical space with a Box filter. The coarse-grained compressible K_{sgs} budget is fully analyzed and the dominant terms are categorized. Current coarse-grained analysis provides a solid basis for the compressible LES modeling in the high Mach number turbulent flow.

This paper is organized as follows. In Section 2, the DNS of supersonic isotropic turbulence by HGKS will be presented. Section 3 presents the transport equation for the compressible SGS turbulent kinetic energy K_{sgs} , and the implementation of coarse-grained analysis on unresolved grids. Conclusion is drawn in the final section.

2. DNS of supersonic isotropic turbulence

The decaying compressible isotropic turbulence is regarded as one of fundamental benchmarks to study the compressible effect [3, 5, 45]. The flow domain of numerical simulation is a cube box defined as $[-\pi, \pi] \times [-\pi, \pi] \times [-\pi, \pi]$, with periodic boundary conditions in all three Cartesian directions for all the flow variables. Evolution of this artificial system is determined by initial thermodynamic quantities and two dimensionless parameters, i.e. the initial Taylor microscale Reynolds number $Re_\lambda = \langle \rho \rangle U_{rms} \lambda / \langle \mu \rangle$ and turbulent Mach number $Ma_t = \sqrt{3} U_{rms} / \langle c_s \rangle$, where $\langle \cdot \rangle$ is the ensemble over the whole computational domain, ρ is the density, λ is the Taylor microscale, μ is the initial dynamic viscosity, c_s is the sound speed and U_{rms} is the root mean square of initial turbulent velocity component $U_{rms} = \langle \mathbf{U} \cdot \mathbf{U} / 3 \rangle^{1/2}$. A three-dimensional solenoidal random initial velocity field \mathbf{U} can be generated by a specified spectrum [46], which is given by

$$E(\kappa) = A_0 \kappa^4 \exp(-2\kappa^2 / \kappa_0^2), \quad (1)$$

where A_0 is a constant to get a specified initial kinetic energy, κ is the wave number, κ_0 is the wave number at which the spectrum peaks. In this paper, fixed A_0 and κ_0 in Eq.(1) are chosen for all cases, which are initialized by $A_0 = 0.00013$ and $\kappa_0 = 8$.

Initial strategies play an important role in compressible isotropic turbulence simulation [45], especially for the starting fast transient period during which the divergence of the velocity increases rapidly and the negative temperature or pressure often appear. In the computation, the initial pressure p_0 , density ρ_0 and temperature T_0 are set as constant. In this way, the initial Taylor microscale Reynolds number Re_λ and turbulent Mach number Ma_t can be determined by

$$Re_\lambda = \frac{(2\pi)^{1/4}}{4} \frac{\rho_0}{\mu_0} \sqrt{2A_0} \kappa_0^{3/2},$$

$$Ma_t = \frac{\sqrt{3}}{\sqrt{\gamma R T_0}} U_{rms},$$

where the initial density $\rho_0 = 1$, μ_0, T_0 can be determined by Re_λ and Ma_t , and $\gamma = 1.4$ is the specific heat ratio. In the simulation, the dynamic viscosity is given by $\mu = \mu_0 (T/T_0)^{0.76}$. With current initial strategy, the initial ensemble turbulent kinetic energy K_0 , ensemble enstrophy Ω_0 , large-eddy-turnover time τ_{to} , ensemble dissipation rate ε_0 , Kolmogorov length scale η_0 , and the Kolmogorov time scale τ_0 are given as

$$K_0 = \frac{3A_0}{64} \sqrt{2\pi} \kappa_0^5, \quad \Omega_0 = \frac{15A_0}{256} \sqrt{2\pi} \kappa_0^7, \quad \tau_{to} = \sqrt{\frac{32}{A_0}} (2\pi)^{1/4} \kappa_0^{-7/2},$$

$$\varepsilon_0 = 2 \frac{\mu_0}{\rho_0} \Omega_0, \quad \eta_0 = (\nu_0^3 / \varepsilon_0)^{1/4}, \quad \tau_0 = (\nu_0 / \varepsilon_0)^{1/2}.$$
(2)

For decaying compressible isotropic turbulence, the root-mean-square pressure fluctuations p_{rms} , and turbulent kinetic energy K are defined as

$$p_{rms} = \sqrt{\langle p - \langle p \rangle \rangle},$$

$$K = \frac{1}{2} \langle \rho \mathbf{U} \cdot \mathbf{U} \rangle.$$
(3)

The evolution of turbulent kinetic energy is of interest since it is a fundamental benchmark for incompressible and compressible turbulence modeling [3, 12, 47]. In this study, the ensemble budget of turbulent kinetic energy is computed and analyzed, as the decay of the ensemble turbulent kinetic energy can be described approximately by [15]

$$\frac{d \langle K \rangle}{dt} = \varepsilon + \langle p \theta \rangle,$$

$$\varepsilon = \varepsilon_s + \varepsilon_d,$$
(4)

where $\varepsilon_s = \langle \mu \omega_i \omega_i \rangle$ is the ensemble solenoidal dissipation rate, $\varepsilon_d = \langle 4\mu\theta^2/3 \rangle$ is the ensemble dilational dissipation rate, $\langle p\theta \rangle$ is the ensemble pressure-dilation transfer, $\omega_i = \epsilon_{ijk} \partial U_k / \partial x_j$ is the fluctuating vorticity, ϵ_{ijk} is the alternating tensor, and $\theta = \nabla \cdot \mathbf{U}$ is the fluctuating divergence of velocity.

In this section, the DNS study of decaying supersonic isotropic turbulence at a fixed

Table 1: Parameters for supersonic isotropic turbulence of R_1 and R_2 .

Test	grid size	Ma_t	Re_λ	$\kappa_{max}\eta_0$	dt_{ini}/τ_{to}
R_1	384^3	2.0	72	2.71	2.00/1000
R_2	512^3	2.0	120	2.80	3.40/1000

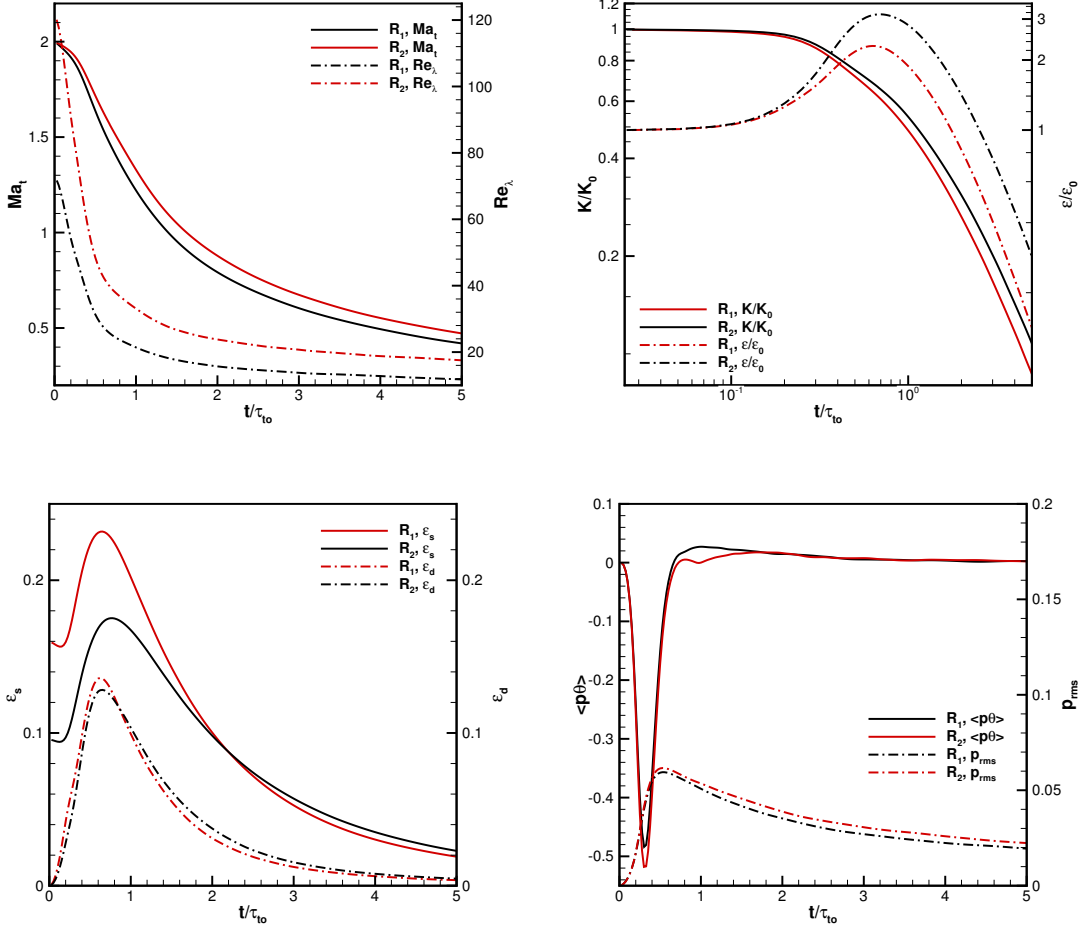


Figure 1: Time history of Ma_t and Re_λ , K/K_0 and $\varepsilon/\varepsilon_0$, ε_s and ε_d , and $\langle p\theta \rangle$ and p_{rms} for cases R_1 and R_2 .

turbulent Mach number $Ma_t = 2.0$ with Taylor microscale Reynolds number $Re_\lambda = 72$ and $Re_\lambda = 120$ are implemented. The grid size and time step are guided by previous criterion of HGKS [8]. The details of numerical tests R_1 and R_2 are given in Table.1, where Δ is the uniform grid size in each direction, $\kappa_{max} = \sqrt{2}\kappa_0 N/3$ is the maximum resolved number wave number [48], $\kappa_0 = 8$ in Eq.(1) and N is the number of grid points in each Cartesian direction. Here dt_{ini} represents the time step for the initial step, and the initial large-eddy turnover time τ_{to} can be determined by Eq.(2). The detailed numerical scheme can be found

in the first part of HGKS for supersonic isotropic turbulence [8, 39, 40].

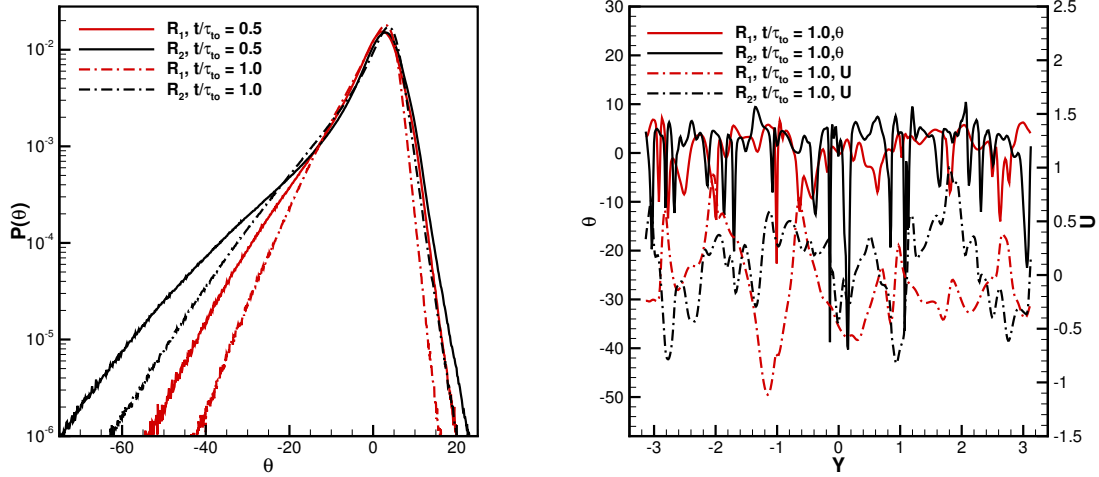


Figure 2: PDF of dilation θ , x -direction velocity component U and dilation θ along $x = 0$ and $z = 0$ at $t/\tau_{to} = 0.5$ and $t/\tau_{to} = 1.0$ for cases R_1 and R_2 .

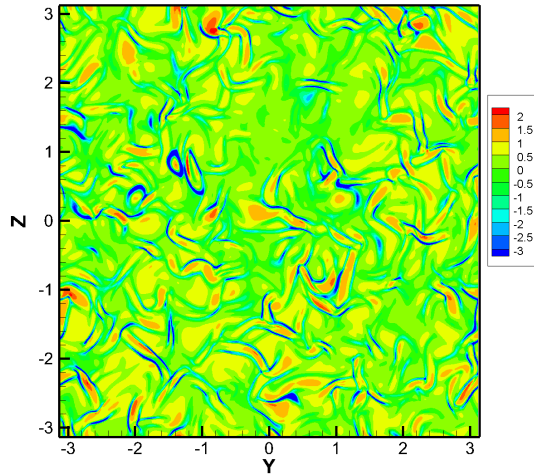


Figure 3: Contour of normalized dilation $\theta / \langle \theta \rangle^*$ at $x = 0$ at $t/\tau_{to} = 0.5$ for case R_1 .

The time history of statistical quantities in Eq.(3) and Eq.(4) are presented in Fig 1. The ensemble turbulent Mach number Ma_t and Taylor microscale Reynolds number Re_λ decay monotonically. During the early stage, Re_λ decays very fast. Up to $t/\tau_{to} = 1.0$, the Taylor microscale Reynolds number Re_λ is approximate 20% of the initial values. Meanwhile, the ensemble dissipation rate ε reaches its maximum, which is around 3 times of ε_0 . Obviously, the peak ensemble dilational dissipation rate ε_d is approximately half of the peak ensemble solenoidal dissipation rate ε_s , which is the significant behavior of high Mach number turbulent flows. Additionally, the ensemble dilational dissipation rate depends on Re_λ slightly, which is confirmed with previous analysis [8]. Root-mean-square pressure fluctuations p_{rms}

reaches its maximum around $t/\tau_{to} = 0.6$, corresponding to the peak ensemble dilational dissipation rate. During the early stage of the decaying supersonic isotropic turbulence, the ensemble pressure-dilation term can be in the same order of ensemble total dissipation rate [45]. The transfer from turbulent kinetic energy to internal energy cannot be neglected as the forced supersonic isotropic turbulence [32]. After $t/\tau_{to} \approx 1.0$, $\langle p\theta \rangle$ changes signs during the evolution and preserves small but positive value.

The probability density functions (PDF) of dilation θ and x -direction velocity component U and dilation θ are presented in Fig.2. All PDFs of dilation θ in Fig.2 are obtained by dividing the dilation range into 1000 equivalent intervals. All PDFs of dilation show strong negative tails, which are the most significant flow structures of compressible isotropic turbulence resulting from the shocklets [7, 8, 9, 10]. The x -direction velocity component U and dilation θ along the $x = 0$ and $z = 0$ indicates that the strong shocklets and high expansion regions appear frequently and randomly. Contour of normalized dilation $\theta/\langle\theta\rangle^*$ at $t/\tau_{to} = 0.5$ of R_1 is presented in Fig.3. Contour of normalized dilation shows very different behavior between the compression motion and expansion motion, where $\langle\theta\rangle^*$ is the root-mean-square dilation. Strong compression regions $\theta/\langle\theta\rangle^* \leq -3$ are usually recognized as shocklets [45]. These random distributed shocklets and high expansion region lead to strong spatial gradient in flow fields, which pose much greater challenge for high-order schemes when implementing DNS for isotropic turbulence in supersonic regime. DNS on a much higher turbulent Mach number up to $Ma_t = 2.0$ has been obtained by HGKS, which confirms the super robustness of HGKS. Based on the high-fidelity DNS data, the coarse-grained analysis for compressible SGS turbulent kinetic energy will be implemented for constructing the compressible one-equation SGS model.

3. Coarse-grained analysis of compressible K_{sgs} budget

In this section, the exact compressible SGS turbulent kinetic energy K_{sgs} transport equation will be derived with density weighted filtering process. The Box filter [49, 50] is used for the coarse-graining processes of compressible K_{sgs} transport equation on three sets of unresolved grids. Finally, the dominant terms in compressible K_{sgs} transport equation are determined for constructing the compressible one-equation SGS model for high turbulent Mach number turbulent flows.

3.1. Compressible K_{sgs} transport equation

For LES models [27, 47], after filtering process on unresolved grids, the flow variables can be decomposed into resolved (filtered) and SGS (residual) terms as follows

$$\phi(\mathbf{x}) = \bar{\phi}(\mathbf{x}) + \phi'(\mathbf{x}). \quad (5)$$

The filtered terms is defined as

$$\bar{\phi}(\mathbf{x}) = \int_{\Omega} G(\mathbf{x}, \mathbf{x}', \mathbf{l}) \phi(\mathbf{x}') d\mathbf{x}',$$

where Ω is the filtered domain and \mathbf{l} denotes the filter width associated with the wavelength of the smallest scale retained by the coarse-graining operation. The filter function G is defined as

$$G(\mathbf{x}, \mathbf{x}', \mathbf{l}) = \prod_i G_i(x_i, x'_i, l_i).$$

The following Box filter [47, 49] in physical space is used in this paper

$$G_i(x_i, x'_i, l_i) = \begin{cases} 1/l_i, & \text{for } |x_i - x'_i| \leq l_i/2, \\ 0, & \text{otherwise,} \end{cases}$$

where l_i is the filter width in i -direction, and the positive definite kernel of Box filter allows positive SGS turbulent kinetic energy [50]. Various filter-widths $l_i = n\Delta_i$ are used in the following analysis, where Δ_i is the i -direction grid size. In current study, the filter width and the grid size are equivalent in x , y and z directions. With the filtered process, the one transport equation K_{sgs} of subgrid-scale kinetic energy for incompressible LES [11, 12] has been derived.

For compressible turbulence modeling, to avoid subgrid term appearing in the filtered continuity equation, the density-weighted (Favre) filtering [51] is applied, which reads

$$\tilde{\phi} = \frac{\overline{\rho\phi}}{\bar{\rho}}. \quad (6)$$

In this way, SGS stress τ_{ij} and SGS kinetic energy $\bar{\rho}K_{sgs}$ are defined as

$$\begin{aligned} \tau_{ij} &= \bar{\rho}(\widetilde{U_i U_j} - \tilde{U}_i \tilde{U}_j), \\ \bar{\rho}K_{sgs} &= \frac{1}{2}\tau_{kk} = \frac{1}{2}\bar{\rho}(\widetilde{U_k U_k} - \tilde{U}_k \tilde{U}_k). \end{aligned} \quad (7)$$

The compressible SGS kinetic energy equation can be derived as Appendix A, the governing equation is given by

$$(\bar{\rho}K_{sgs})_{,t} + (\bar{\rho}K_{sgs}\tilde{U}_j)_{,j} = P_{sgs} - D_{sgs} + \Pi_{sgs} + T_{sgs}, \quad (8)$$

where P_{sgs} is the SGS production term, D_{sgs} is the SGS dissipation term, Π_{sgs} is the SGS pressure dilation term, and the last term T_{sgs} is the sum of SGS diffusion terms. More specifically, the right-hand-side terms in Eq.(8) can be written as

$$\begin{aligned} P_{sgs} &= -\tau_{ij}\tilde{S}_{ij}, \\ D_{sgs} &= \overline{\sigma_{ij}U_{i,j}} - \bar{\sigma}_{ij}\tilde{U}_{i,j}, \\ \Pi_{sgs} &= \overline{pU_{k,k}} - \bar{p}\tilde{U}_{k,k}, \\ T_{sgs} &= [-\frac{1}{2}\bar{\rho}(\widetilde{U_i U_i U_j} - \widetilde{U_i U_i} \tilde{U}_j) + \tau_{ij}\tilde{U}_i + (\overline{\sigma_{ij}U_i} - \bar{\sigma}_{ij}\tilde{U}_i) - \bar{\rho}R(\widetilde{TU_j} - \tilde{T}\tilde{U}_j)]_{,j}, \end{aligned} \quad (9)$$

where $\tilde{S}_{ij} = 1/2(\tilde{U}_{i,j} + \tilde{U}_{j,i})$. More details about the derivation of Eq.(8) can be found in Appendix A. The SGS production term $-\tau_{ij}\tilde{S}_{ij}$ represents the inter-scale transfer associated with the interaction of the resolved and unresolved scales. There exists local SGS turbulent kinetic energy backscatter, which illustrates the SGS turbulent kinetic energy transfer from sub-grid scales to resolved scales [32, 49]. As presented in Appendix A, the total SGS dissipation rate D_{sgs} can be decomposed into two parts, the SGS solenoidal dissipation rate ε_s^{sgs} and SGS dilational dissipation rate ε_d^{sgs} , as

$$\begin{aligned}\varepsilon_s^{sgs} &= \bar{\mu}(\widetilde{\omega_i\omega_i} - \tilde{\omega}_i\tilde{\omega}_i), \\ \varepsilon_d^{sgs} &= 4\bar{\mu}(\widetilde{U_{k,k}^2} - \tilde{U}_{k,k}^2)/3,\end{aligned}\tag{10}$$

where $\omega_i = \epsilon_{ijk}U_{k,j}$ is the resolved vorticity and $\tilde{\omega}_i = \epsilon_{ijk}\tilde{U}_{k,j}$ is the unresolved one with the alternating tensor ϵ_{ijk} . There is a slight difference between Eq.(10) and Eq.(3.8) in the reference [25]. Restricting the analysis to the linear Kovasznay splitting [52], the solenoidal dissipation is associated entirely with the vorticity mode, whereas the dilational dissipation is mainly due to the acoustic mode in the absence of significant entropy source [5]. Π_{sgs} is SGS pressure-dilation term, which is related to the redistribute K_{sgs} in the flowfields for compressible turbulence. The SGS pressure-dilation term reduce to 0 in the incompressible limit. T_{sgs} is the sum of all SGS diffusion terms, which are usually grouped and modeled together both for incompressible and compressible turbulence models [6, 21]. In this paper, to determine the dominant SGS diffusion term, all SGS diffusion terms are analyzed in detail.

According to the Eq.(9), the right-hand-side terms of Eq.(8) are classified as Table.2. With the Favre filtering process on unresolved grids, the analysis of dominant source terms and SGS diffusion terms will be presented in the following section.

Table 2: Expressions for the right-hand-side terms in compressible K_{sgs} equation.

Symbol	Expression	Symbol	Expression
P	$-\tau_{ij}\tilde{S}_{ij}$	T_1	$[-\frac{1}{2}\bar{\rho}(\widetilde{U_iU_iU_j} - \tilde{U}_i\tilde{U}_i\tilde{U}_j)]_{,j}$
D_1	$\bar{\mu}(\widetilde{\omega_i\omega_i} - \tilde{\omega}_i\tilde{\omega}_i)$	T_2	$(\tau_{ij}\tilde{U}_i)_{,j}$
D_2	$4\bar{\mu}(\widetilde{U_{k,k}^2} - \tilde{U}_{k,k}^2)/3$	T_3	$[(\overline{\sigma_{ij}U_i} - \bar{\sigma}_{ij}\tilde{U}_i)]_{,j}$
Π	$\overline{pU_{k,k}} - \bar{p}\tilde{U}_{k,k}$	T_4	$[-\bar{\rho}R(\widetilde{TU_j} - \tilde{T}\tilde{U}_j)]_{,j}$

3.2. Coarse-grained analysis of compressible K_{sgs} transport equation

The DNS and filtering LES grids for R_1 and R_2 are presented in Table.3. The discretization method of spatial derivatives plays a key role in analyzing the budget of compressible K_{sgs} transport equation. In current paper, to be consistent with HGKS calculation [8], the fifth-order WENO-Z reconstruction [53] is adopted in computing the spatial derivatives of flow variables, and details are given in Appendix B.

Table 3: DNS and filtering LES grids for R_1 and R_2

	grid size	$\kappa_{max}\eta_0$		grid size	$\kappa_{max}\eta_0$
DNS	384^3	2.71	DNS	512^3	2.80
case A_1	192^3	1.36	case B_1	256^3	1.40
case A_2	96^3	0.68	case B_2	128^3	0.70
case A_3	64^3	0.45	case B_3	64^3	0.35

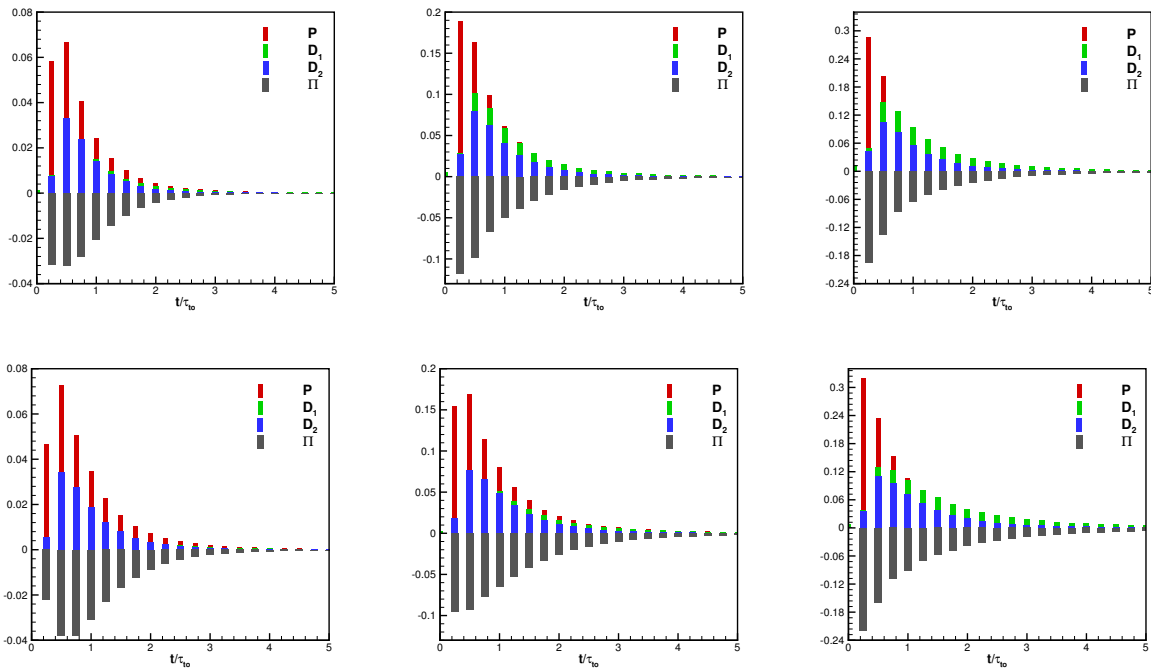


Figure 4: Coarse-grained compressible K_{sgs} budgets of P , D_1 , D_2 , and Π for cases A_1 , A_2 , A_3 (upper row) and B_1 , B_2 , B_3 (lower row).

The coarse-grained compressible K_{sgs} budgets P , D_1 , D_2 and Π in Eq.(9) for cases A_1 - A_3 and B_1 - B_3 are presented as the Fig.4. The budgets are computed in the ensemble norm, and the spatial derivatives are obtained by WENO-Z reconstruction as the Appendix B. The ensemble norm is defined as $\|x\| = \sum_{i=1}^N x_i/N$. As shown in Fig.4, all unresolved source terms are dominant terms within the $0 \leq t/\tau_{to} \leq 3.0$. Obviously, the SGS production term $-\tau_{ij}\widetilde{S}_{ij}$ is the most important term, considering the largest positive magnitude among the four source terms. The ensemble P is positive, which represents the ensemble SGS kinetic energy forward scatter. The ensemble SGS dilational dissipation rate D_2 is more than half of the ensemble SGS solenoidal dissipation rate D_1 . Compared with the incompressible turbulence system, the dilational dissipation rate cannot be neglected in supersonic turbulence. The coarse-grained analysis on SGS dissipation rate for supersonic isotropic turbulence agrees with previous conclusion on compressible turbulence at a moderate turbulent Mach number ($Ma_t = 0.52$) [31]. In addition, with the coarser grids, the ratio of the

D_2 to D_1 becomes larger. When modeling the SGS dissipation rate, the one-equation SGS model for compressible LES should consider the grids effect [23, 24, 25]. The negative values of Π represents the ensemble SGS pressure-dilation term acts as the sink for SGS kinetic energy. Different with the Fig.1, the SGS pressure-dilation term Π doesn't change signs during the evolution and always preserves negative value on unresolved grids. Especially, the magnitude of SGS pressure-dilation term Π is in the order of unresolved SGS dissipation term within the acoustic time scale τ_a , where acoustic time is defined as $\tau_a = Ma_t \tau_{to}$ [4]. Thus, for decaying supersonic isotropic turbulence, it can be concluded that the SGS pressure-dilation term cannot be neglected as previous comments [23, 32]. The literature for modeling SGS pressure-dilation term in subsonic regime can be found in Refs [16, 17, 20], while it is still required to be studied for supersonic isotropic turbulence. When $t/\tau_{to} \geq 3.0$, from Fig.1, the turbulent Mach number $Ma_t \approx 0.7$ and Taylor microscale Reynolds number $Re_\lambda \leq 20$, the resolved ensemble dissipation rate and pressure-dilation rate decrease to a small magnitude. At the same time, on unresolved grids as Fig.4, the source terms decay to a very small magnitude, which indicate that even the coarsest grids A_3 and B_3 are fine enough to resolve the flowfields. This behavior is reasonable since the current system experience a very small Taylor microscale Reynolds number $Re_\lambda \leq 20$.

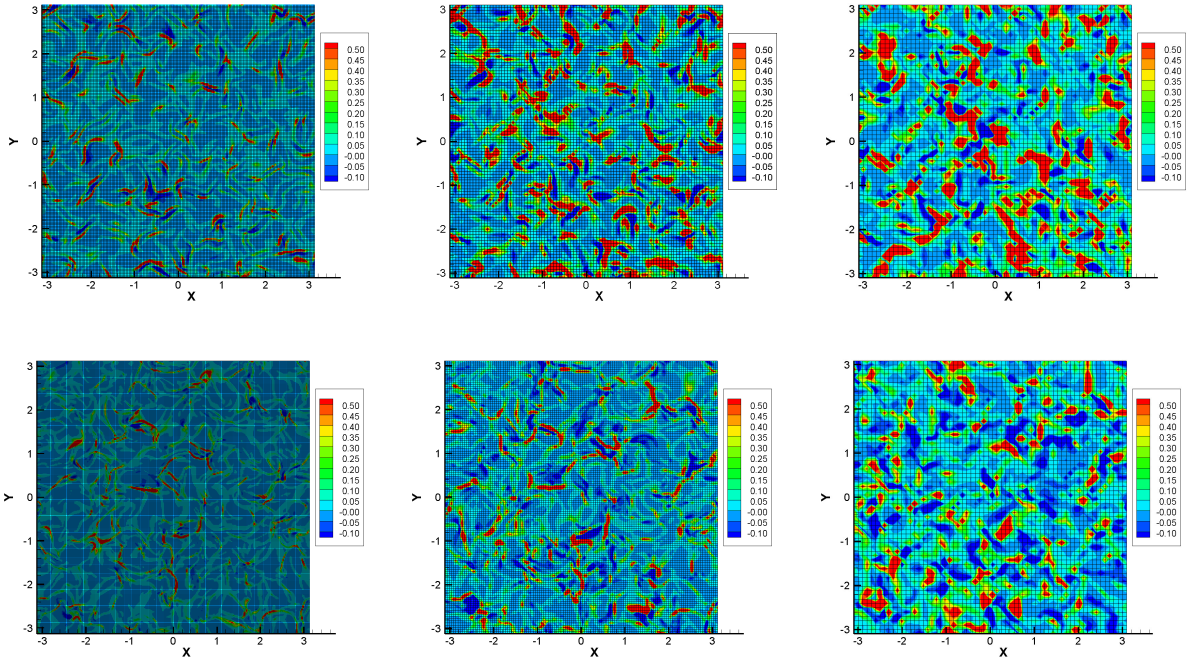


Figure 5: SGS production term P for cases A_1 , A_2 and A_3 at $t/\tau_{to} = 0.5$ at $z = 0$ (upper row), and cases B_1 , B_2 and B_3 at $t/\tau_{to} = 1.0$ at $z = 0$ (lower row).

The contours of SGS production term P for cases A_1 - A_3 at $t/\tau_{to} = 0.5$ and B_1 - B_3 at $t/\tau_{to} = 1.0$ at $z = 0$ are presented in Fig.5. The forward scatter and backscatter coexist [49, 32] and randomly distribute on the unresolved grids. It can be seen that the magnitude and portion of positive $-\tau_{ij}\widetilde{S}_{ij}$ is larger than the negative ones, confirming that the ensemble

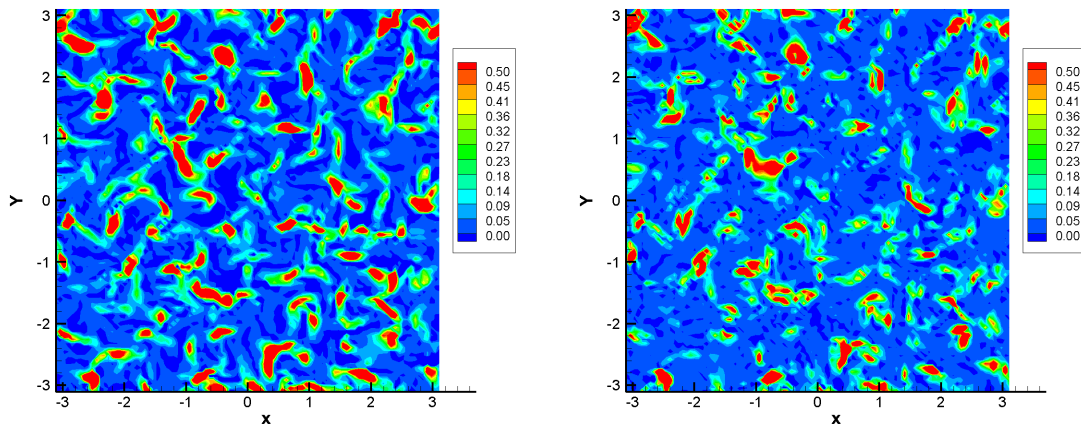


Figure 6: SGS solenoidal dissipation term D_1 (left), SGS dilational dissipation term D_2 (right) for case A_2 at $t/\tau_{to} = 0.5$ at $z = 0$.

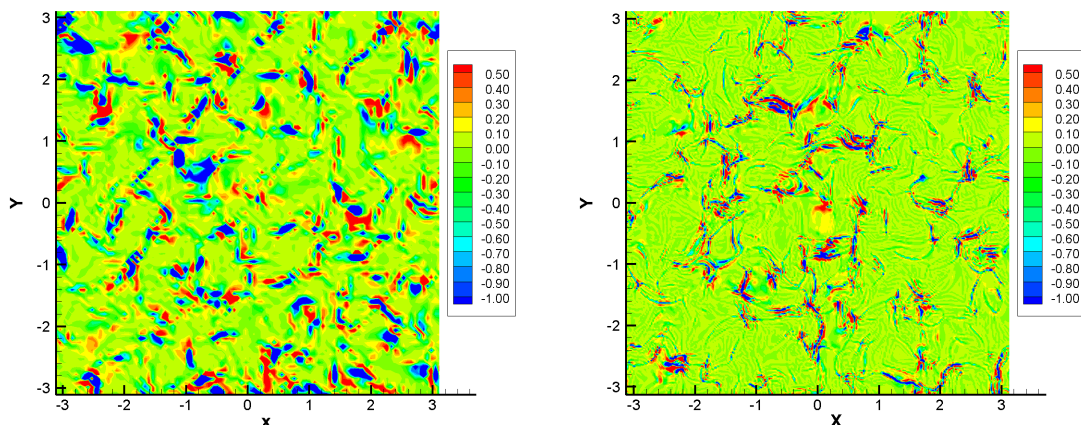


Figure 7: SGS pressure-dilation transfer term Π for case A_2 at $t/\tau_{to} = 0.5$ (left) and B_1 at $t/\tau_{to} = 1.0$ (right) at $z = 0$.

forward scatter transfers the SGS turbulent kinetic energy from the resolved scales to the sub-grid scales. To model the backscatter process in supersonic isotropic turbulence, the dynamic approach is recommended [25, 54]. Contours of SGS solenoidal dissipation term D_1 , dilational dissipation term D_2 for case A_2 at $t/\tau_{to} = 0.5$ and B_1 at $t/\tau_{to} = 1.0$ at $z = 0$ are presented as that in Fig.6. The dissipation rate is non-negative, and the high similarity between the D_1 and D_2 in spatial distribution are confirmed [25]. Previous modeling [15] on dilational dissipation rate $D_2 \propto Ma_t^2 D_1$ may still work in this supersonic isotropic turbulence, which will be studied in the following paper. Figure 7 shows the SGS pressure-dilation transfer term Π for case A_2 at $t/\tau_{to} = 0.5$ and B_1 at $t/\tau_{to} = 1.0$ at $z = 0$. It can be seen that the magnitude and portion of negative Π is larger than the positive ones, which confirms the ensemble SGS pressure-dilation term absorbing the K_{sgs} as Fig.4.

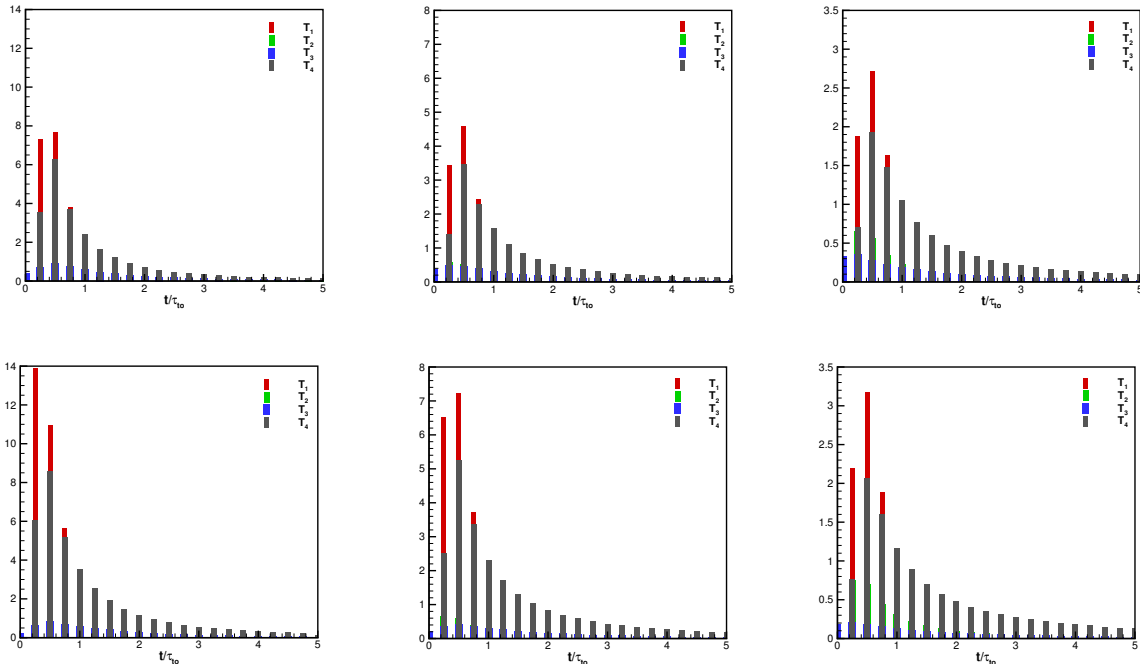


Figure 8: Coarse-grained budgets of SGS diffusion terms T_1 , T_2 , T_3 and T_4 for cases A_1 , A_2 , A_3 (upper row) and B_1 , B_2 , B_3 (lower row).

In previous study, the SGS diffusion terms are grouped and modeled together by the gradient-type models for both incompressible and compressible turbulent flows [6, 21]. To study the delicate behavior of SGS diffusion terms in SGS kinetic energy equation, the coarse-grained analysis of dominant SGS diffusion terms is implemented. Coarse-grained budget of SGS diffusion terms T_1 , T_2 , T_3 and T_4 for case A_1 - A_3 and B_1 - B_3 are presented as the Fig.8. The budgets are computed in the L_2 norm, and the spatial derivatives are obtained by WENO-Z reconstruction as the Appendix B. Because the ensemble of the sum of transport terms is equivalent to 0, the L_2 norm is applied in analyzing the SGS diffusion terms. The L_2 norm is defined as $\|x\|_{L_2} = (\sum_{i=1}^N x_i^2)^{0.5}/N$. As shown in Fig.8, within the $0 \leq t/\tau_{to} \leq 2.0$, both the fluctuation velocity triple correlation term T_1 and the pressure-velocity correlation term T_4 are dominant terms. T_1 and T_4 are about 10 times larger than the negligible terms T_2 and T_3 , i.e., $\|T_1\|_{L_2} \approx 10\|T_4\|_{L_2}$. The coarse-grained analysis on SGS diffusion terms for supersonic isotropic turbulence agrees with previous conclusion on subsonic isotropic turbulence [29], i.e., priori tests of a mixing layer up to Mach numbers 0.6. When $t/\tau_{to} \geq 3.0$, all SGS diffusion terms T_1 - T_4 decay to a very small magnitude similar as Fig.4. This is because of the very small Taylor microscale Reynolds number $Re_\lambda \leq 20$, even the coarsest grids A_3 and B_3 are fine enough to resolve the flowfields.

The contours of SGS diffusion terms T_1 , T_2 , T_3 and T_4 for case A_2 at $t/\tau_{to} = 0.5$ are presented in Fig.9, in which the fluctuation velocity triple correlation term T_1 and the pressure-velocity correlation term T_4 behave more importantly than the SGS diffusion term T_2 and T_3 . To be of interest, the fluctuation velocity triple correlation term T_1 and the

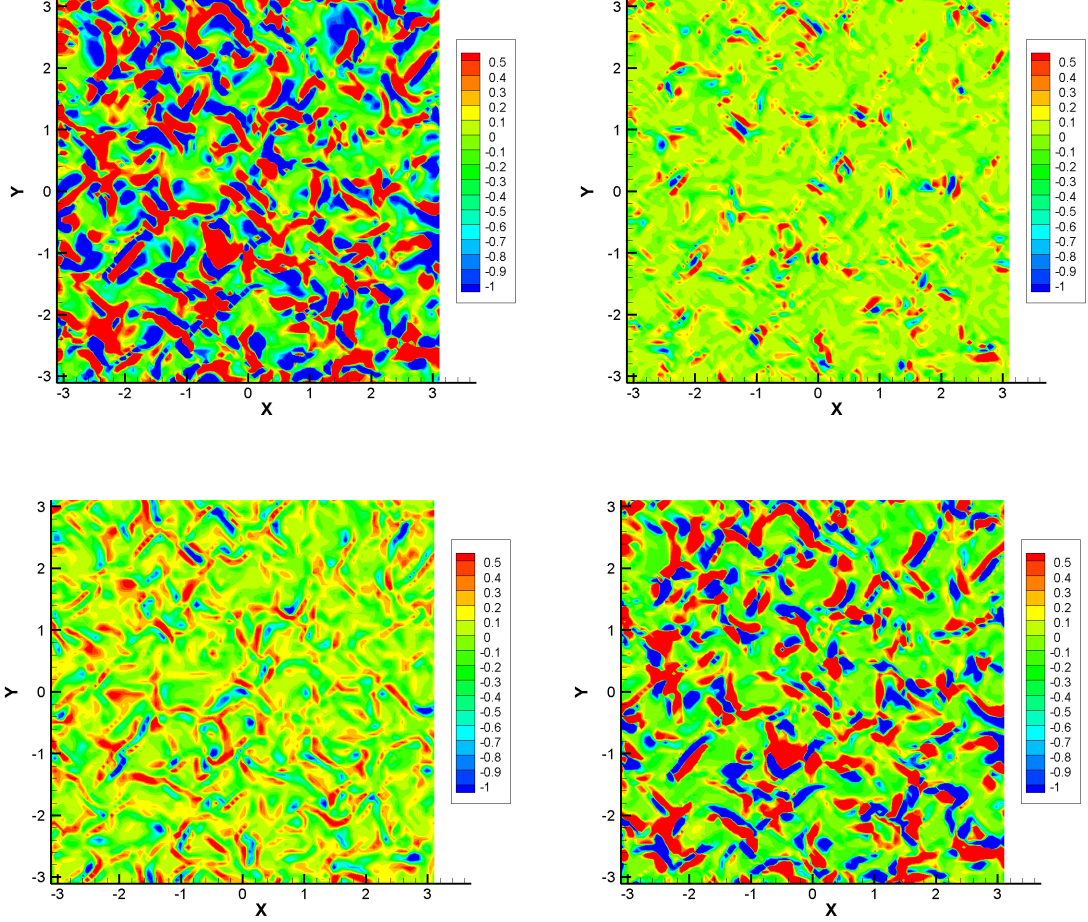


Figure 9: SGS diffusion terms T_1 , T_2 (upper row), T_3 and T_4 (lower row) diffusion terms for case A_2 at $t/\tau_{to} = 0.5$ at $z = 0$.

pressure-velocity correlation term T_4 are found to be highly correlated. To further study the correlation, KullbackLeibler divergence (KLD) [55] is introduced to measure the relationship of statistical behavior, namely, the correlation between two PDFs of SGS diffusion term. In addition, the linear correlation coefficient is used to measure the spatial correlation of four SGS diffusion terms. The KLD and linear correlation coefficient are defined as

$$\begin{aligned}
 D_{kl}(\mathbf{T}_i || \mathbf{T}_1) &= \sum_i \mathbf{T}_i(i) \log \frac{\mathbf{T}_i(i)}{\mathbf{T}_1(i)}, \\
 Coe(\mathbf{T}_i || \mathbf{T}_1) &= \frac{\text{cov}(\mathbf{T}_i, \mathbf{T}_1)}{\sigma_{\mathbf{T}_i} \sigma_{\mathbf{T}_1}},
 \end{aligned} \tag{11}$$

where \mathbf{T}_i is the PDF of SGS diffusion term T_i , and all PDFs of T_i in this paper are obtained by dividing the SGS diffusion term range into 1000 equivalent intervals. $\text{cov}(\cdot, \cdot)$ represents the covariance of two random variables, and σ is standard deviation of one random variables.

History of KLD and linear correlation coefficient among the SGS diffusion terms T_1 , T_2 , T_3 and T_4 for case B_1 - B_3 are presented as Fig.10. The coarser grid is, the smaller magnitude of KLD is, indicating the closer relation between T_i and T_1 . As different grids show different order of magnitude of KLD, it indicates that the grid effect should be considered for constructing the one-equation SGS model. The linear correlation coefficient confirms the high correlation between T_1 and T_4 , which indicates the strong coupling between the kinematics and thermodynamics in current supersonic isotropic turbulence. When using the dynamic approach [28] to determine the dynamic coefficients for modeling SGS diffusion term [25], both T_1 and T_4 should participate in the dynamic approach, instead of only considering T_1 as incompressible one-equation SGS model [13, 14].

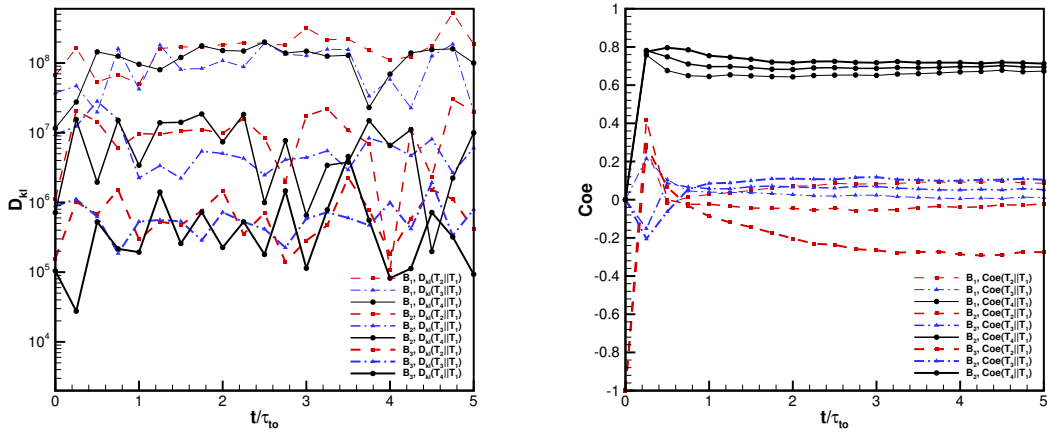


Figure 10: History of Kullback-Leibler divergence (left) and linear correlation coefficient (right) among the SGS diffusion terms T_1 , T_2 , T_3 and T_4 for cases B_1 - B_3 .

Table 4: Classification of terms in incompressible and compressible K_{sgs} equation.

Category	Current compressible system	Incompressible system
Dominant terms	$P, D_1, D_2, \Pi, T_1, T_4$	P, D_1, T_1
Negligible terms	T_2, T_3	D_2, Π, T_2, T_3, T_4

In summary, the classification of terms in the compressible K_{sgs} equation are presented in Table.4. Compared with incompressible turbulent system [11], current study points out the additional dominant terms D_2 , Π and T_4 , which deserves further study for high Mach number turbulence modeling. Compressible K_{sgs} transport equation is analyzed, which paves the way for modeling the unknowns in compressible one-equation SGS model. Subsequent paper will focus on the compressible one-equation SGS model for high turbulent Mach number turbulent flows.

4. Conclusion

In this paper, the coarse-grained analysis of compressible SGS turbulent kinetic energy budget K_{sgs} is fully analyzed for constructing one-equation SGS model of compressible LES at high turbulent Mach number. DNS on a much higher turbulent Mach number up to $Ma_t = 2.0$ has been obtained by HGKS, which provides the high-fidelity DNS data for coarse-grained analysis. The exact compressible SGS turbulent kinetic energy K_{sgs} transport equation is also derived with Favre filtering process. Based on the compressible K_{sgs} transport equation, the coarse-graining processes are implemented on unresolved grids. The coarse-grained analysis of compressible K_{sgs} budgets shows that all unresolved source terms are dominant terms, i.e., the SGS production term, the SGS solenoidal dissipation term, the SGS dilational dissipation term, and the SGS pressure-dilation term. Especially, for the decaying supersonic isotropic turbulence, the SGS pressure-dilation term plays the significant role in SGS turbulent kinetic energy transfer, which cannot be neglected. The coarse-grained analysis of SGS diffusion terms in compressible K_{sgs} budgets shows both the fluctuation velocity correlation term and the pressure-velocity correlation term are dominant terms. The pressure-velocity correlation term should participate in the dynamic approach when determining the dynamic coefficients for modeling SGS diffusion term. The current coarse-grained analysis gives an indication of the order of magnitude of all unresolved terms in compressible K_{sgs} budget, which provides a solid basis for compressible one-equation SGS model. The compressible one-equation SGS model within the non-equilibrium time-relaxation kinetic framework for high turbulent Mach number turbulence will be presented in the subsequent paper.

Acknowledgement

The current research is supported by National Science Foundation of China (11701038, 11772281, 91852114), the Fundamental Research Funds for the Central Universities (2018NTST19), and the National Numerical Windtunnel project. The authors would like to thank TianHe-II in Guangzhou for providing high performance computational resources.

Appendix A: derivation of compressible K_{sgs} transport equation

For the filtering operator as Eq.(5), the following two properties, namely linearity and commutation with differentiation [47] are required as

$$\begin{aligned} \overline{\phi + \varphi} &= \overline{\phi} + \overline{\varphi}, \\ \overline{\frac{\partial \phi}{\partial s}} &= \frac{\partial \overline{\phi}}{\partial s}, \end{aligned} \tag{12}$$

where $s = \mathbf{x}, t$. To avoid subgrid term appearing in the filtered continuity equation, the Favre filtering [51] as Eq.(6) is considered. For Favre filtering, only the linearity has been inherited as

$$\widetilde{\phi + \varphi} = \widetilde{\phi} + \widetilde{\varphi}. \tag{13}$$

It should be noticed that the commutation with differentiation don't apply to the Favre filtering. The SGS kinetic energy equation can be derived by subtracting the product of the Favre-filtered velocity and the filtered momentum equation from the filtered product of the velocity and momentum equation [25]

$$\overline{U_i \times [(\rho U_i)_t + (\rho U_i U_j)_j + p_i - (\sigma_{ij})_j]} - \widetilde{U}_i \times \overline{(\rho U_i)_t + (\rho U_i U_j)_j + p_i - (\sigma_{ij})_j} = 0, \quad (14)$$

where ρ is the density, U_i is the velocity component, $p = \rho RT$ is the pressure, and T is the temperature and R is the gas constant. Ignoring the bulk viscosity, the viscous stress σ_{ij} is given by

$$\sigma_{ij} = \mu(U_{i,j} + U_{j,i} - \frac{2}{3}U_{k,k}\delta_{ij}),$$

where μ is the molecular viscosity, and δ_{ij} is the Kronecker symbol. Based on properties of filtered process as Eq.(12) and Eq.(13), Eq.(14) can be rearranged term by term to derive SGS kinetic energy equation.

The first term L_1 is defined and grouped as

$$L_1 = \overline{U_i \times (\rho U_i)_t} - \widetilde{U}_i \times \overline{(\rho U_i)_t} = [\overline{\rho(\widetilde{U}_i \widetilde{U}_i - \widetilde{U}_i \widetilde{U}_i)}]_t - (\overline{\rho U_i U_{i,t}} - \overline{\rho \widetilde{U}_i \widetilde{U}_{i,t}}). \quad (15)$$

The continuity and momentum equation can be used to replace $U_{i,t}$ as $\rho U_{i,t} = (\rho U_i)_t - U_i \rho_t$. Similarly, the filtered continuity equation and filtered momentum equation can be used to replace $\widetilde{U}_{i,t}$. Plugging above replacements into Eq.(15), L_1 can be rewritten as

$$L_1 = [\overline{\rho(\widetilde{U}_i \widetilde{U}_i - \widetilde{U}_i \widetilde{U}_i)}]_t + \overline{U_i \times [(\rho U_i U_j)_j + p_i - (\sigma_{ij})_j]} - \widetilde{U}_i \times \overline{(\rho U_i U_j)_j + p_i - (\sigma_{ij})_j} - [\overline{U_i^2 (\rho U_j)_j} - \widetilde{U}_i^2 (\overline{\rho \widetilde{U}_j})_j].$$

With the definition of SGS kinetic energy $\overline{\rho(\widetilde{U}_k \widetilde{U}_k - \widetilde{U}_k \widetilde{U}_k)} = 2\overline{\rho K_{sgs}}$ in Eq.(7), plugging L_1 into Eq.(14), leads to

$$2(\overline{\rho K_{sgs}})_t + 2 \left\{ \overline{U_i \times [(\rho U_i U_j)_j + p_i - (\sigma_{ij})_j]} - \widetilde{U}_i \times \overline{(\rho U_i U_j)_j + p_i - (\sigma_{ij})_j} \right\} = \overline{U_i^2 (\rho U_j)_j} - \widetilde{U}_i^2 (\overline{\rho \widetilde{U}_j})_j. \quad (16)$$

The second term L_2 can be defined and rewritten as

$$L_2 = \overline{U_i \times (\rho U_i U_j)_j} - \widetilde{U}_i \times \overline{(\rho U_i U_j)_j} = \overline{(\rho U_i U_i U_j)_j - \rho U_i U_j U_{i,j}} - \widetilde{U}_i \times [(\overline{\rho \widetilde{U}_i \widetilde{U}_j})_j + (\tau_{ij})_j], \quad (17)$$

where $\tau_{ij} = \overline{\rho(\widetilde{U}_i \widetilde{U}_j - \widetilde{u}_i \widetilde{u}_j)}$ as defined in Eq.(7). Combining L_2 and the right-hand-side term in Eq.(16), we have

$$L_3 = 2 \times L_2 - [\overline{U_i^2 (\rho U_j)_j} - \widetilde{U}_i^2 (\overline{\rho \widetilde{U}_j})_j] = 2(\overline{\rho K_{sgs}} \widetilde{U}_j)_j + [\overline{\rho(\widetilde{U}_i \widetilde{U}_i \widetilde{U}_j - \widetilde{U}_i \widetilde{U}_i \widetilde{U}_j)}]_j - 2\widetilde{U}_i (\tau_{ij})_j.$$

The last term in L_3 can be rewritten as

$$\widetilde{U}_i(\tau_{ij})_{,j} = (\tau_{ij}\widetilde{U}_i)_{,j} - \tau_{ij}\widetilde{U}_{i,j} = (\tau_{ij}\widetilde{U}_i)_{,j} - \tau_{ij}\widetilde{S}_{ij},$$

where the decomposition $\widetilde{U}_{i,j} = \widetilde{S}_{ij} + \widetilde{\Omega}_{ij}$ is involved, $\widetilde{S}_{ij} = (\widetilde{U}_{i,j} + \widetilde{U}_{j,i})/2$ and $\widetilde{\Omega}_{ij} = (\widetilde{U}_{i,j} - \widetilde{U}_{j,i})/2$. $\tau_{ij}\widetilde{\Omega}_{ij} = 0$ because it involves multiplication of a symmetric tensor τ_{ij} by an anti-symmetric tensor $\widetilde{\Omega}_{ij}$. Plug L_3 into Eq.(16), which leads to

$$\begin{aligned} 2(\overline{\rho K_{sgs}})_{,t} + 2(\overline{\rho K_{sgs}\widetilde{U}_j})_{,j} + 2\left\{\overline{U_i \times [p_{,i} - (\sigma_{ij})_{,j}]} - \widetilde{U}_i \times \overline{p_{,i} - (\sigma_{ij})_{,j}}\right\} \\ = -2\tau_{ij}\widetilde{S}_{ij} - [\overline{\rho(\widetilde{U}_i\widetilde{U}_i\widetilde{U}_j - \widetilde{U}_i\widetilde{U}_i\widetilde{U}_j)}]_{,j} + 2(\tau_{ij}\widetilde{U}_i)_{,j}. \end{aligned} \quad (18)$$

In Eq.(18), substituting $\bar{p} = \bar{\rho}R\tilde{T}$ into pressure-gradient velocity correlation, leads to the following form

$$L_4 = \overline{U_i \times p_{,i}} - \widetilde{U}_i \times \overline{p_{,i}} = [\bar{\rho}R(\overline{\widetilde{T}U_i} - \widetilde{T}\widetilde{U}_i)_{,i} - (\overline{pU_{i,i}} - \widetilde{p}\widetilde{U}_{i,i})].$$

The term L_5 can be designed and decomposed as follows

$$\begin{aligned} L_5 &= \overline{U_i \times (\sigma_{ij})_{,j}} - \widetilde{U}_i \times \overline{(\sigma_{ij})_{,i}} \\ &= (\overline{\sigma_{ij}U_i} - \overline{\sigma_{ij}\widetilde{U}_i})_{,j} - (\overline{\sigma_{ij}U_{i,j}} - \overline{\sigma_{ij}\widetilde{U}_{i,j}}), \end{aligned}$$

Plugging L_4 and L_5 into Eq.(18), the SGS kinetic energy equation reads

$$\begin{aligned} (\overline{\rho K_{sgs}})_{,t} + (\overline{\rho K_{sgs}\widetilde{U}_j})_{,j} &= -\tau_{ij}\widetilde{S}_{ij} - (\overline{\sigma_{ij}U_{i,j}} - \overline{\sigma_{ij}\widetilde{U}_{i,j}}) + (\overline{pU_{k,k}} - \widetilde{p}\widetilde{U}_{k,k}) \\ &+ [-\frac{1}{2}\overline{\rho(\widetilde{U}_i\widetilde{U}_i\widetilde{U}_j - \widetilde{U}_i\widetilde{U}_i\widetilde{U}_j)} + \tau_{ij}\widetilde{U}_i + (\overline{\sigma_{ij}U_i} - \overline{\sigma_{ij}\widetilde{U}_i}) - \bar{\rho}R(\overline{\widetilde{T}U_j} - \widetilde{T}\widetilde{U}_j)]_{,j}. \end{aligned} \quad (19)$$

In practice, two assumptions are introduced to decompose the total SGS dissipation rate into SGS solenoidal part and SGS dilational one. Firstly, assume that the kinematic viscosity ν is spatially uniform over the filter width, so that $\overline{\mu\phi} = \bar{\rho}\nu\tilde{\phi} = \bar{\mu}\tilde{\phi}$. In addition, for compressible turbulence, the assumption $\overline{\sigma_{ij}} = 2\bar{\mu}(\widetilde{S}_{ij} - \delta_{ij}\widetilde{S}_{kk}/3)$ is adopted in previous literature [29, 31]. Then, the total SGS dissipation rate ε^{sgs} in Eq.(19) can be rewritten as

$$\begin{aligned} \varepsilon^{sgs} &= \overline{\sigma_{ij}U_{i,j}} - \overline{\sigma_{ij}\widetilde{U}_{i,j}} \\ &= 2\bar{\mu}(\overline{\widetilde{S}_{ij}U_{i,j}} - \widetilde{S}_{ij}\widetilde{U}_{i,j}) - 2\bar{\mu}(\overline{U_{k,k}^2} - \widetilde{U}_{k,k}^2)/3. \end{aligned}$$

Using the fact $S_{ij}S_{ij} = \omega_i\omega_i/2 + U_{i,j}U_{j,i}$, the total dissipation rate ε^{sgs} could be decomposed into SGS solenoidal dissipation rate ε_s^{sgs} and SGS dilational dissipation rate ε_d^{sgs} as follow

$$\begin{aligned} \varepsilon_s^{sgs} &= \bar{\mu}(\overline{\widetilde{\omega}_i\widetilde{\omega}_i} - \widetilde{\omega}_i\widetilde{\omega}_i), \\ \varepsilon_d^{sgs} &= 2\bar{\mu}(\overline{U_{i,j}U_{j,i}} - \widetilde{U}_{i,j}\widetilde{U}_{j,i}) - 2\bar{\mu}(\overline{U_{k,k}^2} - \widetilde{U}_{k,k}^2)/3, \end{aligned} \quad (20)$$

where $\omega_i = \epsilon_{ijk} U_{k,j}$ is the vorticity and $\tilde{\omega}_i = \epsilon_{ijk} \tilde{U}_{k,j}$, with the alternating tensor ϵ_{ijk} . With the reasonable assumption $U_{i,j} U_{j,i} \approx U_{k,k}^2$ [21] (exactly in homogeneous turbulence), the SGS dilational dissipation rate ε_d^{sgs} in Eq.(20) can be approximated as

$$\varepsilon_d^{sgs} = 4\bar{\mu}(\widetilde{U_{k,k}^2} - \tilde{U}_{k,k}^2)/3. \quad (21)$$

The difference between current derivation on dissipation rate as Eq.(20) and Eq.(21) and the reference literature [25] as Eq.(3.4), Eq.(3.5) and Eq.(3.8) should be pointed out. In the reference [25], Eq.(3.4) represents the total dissipation rate instead of the solenoidal dissipation rate.

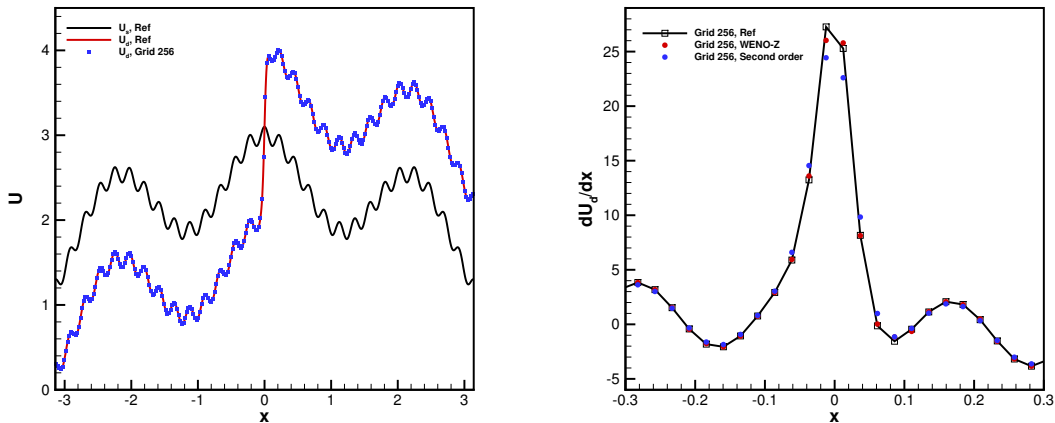


Figure 11: Initial wave of $U_s(x)$ and $U_d(x)$, and spatial derivative of $U_d(x)$ with the analytical solution, fifth-order WENO-Z reconstruction, and second-order central difference method.

Table 5: Accuracy test of spatial derivative for $U_s(x)$ and $U_d(x)$ with WENO-Z reconstruction.

Waves	$U_s(x)$		$U_d(x)$	
Mesh length	L^2 error	Order	L^2 error	Order
$2\pi/64$	$2.619209e - 01$		$3.458353e - 01$	
$2\pi/128$	$3.050078e - 02$	3.10	$4.959606e - 02$	2.81
$2\pi/256$	$3.088122e - 03$	4.62	$6.520176e - 03$	4.14
$2\pi/512$	$6.699721e - 05$	3.98	$4.571909e - 04$	3.19

Appendix B: spatial derivatives in consistent with numerical scheme

The one-dimensional multiple-frequency smooth wave $U_s(x)$ as well as the waves with sharp derivative $U_d(x)$ are used to test the accuracy of spatial derivative. The sharp derivative is designed for simulating the shocklets as shown in Fig.2. The $U_s(x)$ and $U_d(x)$ are

given by

$$\begin{aligned}
 U_s(x) &= \sum_{i=1}^3 \alpha_i \cos(2\beta_i \pi x), x \in [-\pi, \pi], \\
 U_d(x) &= \sum_{i=1}^3 \alpha_i \cos(2\beta_i \pi x) + \tanh(\gamma x), x \in [-\pi, \pi],
 \end{aligned}
 \tag{22}$$

where the coefficients $\alpha_1 = 800, \alpha_2 = 80, \alpha_3 = 8$ and $\beta_1 = 0.1, \beta_2 = 0.5, \beta_3 = 2.5, \gamma = 30$ are adopted. Initial waves of $U_s(x)$ and $U_d(x)$ are presented in Figure 11. Three methods are used to compute the spatial derivative, namely the analytical solution, fifth-order WENO-Z reconstruction [53], and second-order central difference method. Compared with the analytic solution, the fifth-order WENO-Z reconstruction outweighs the second-order central difference method. In current paper, WENO-Z reconstruction is applied to compute the spatial derivative. The accuracy tests of $U_s(x)$ and $U_d(x)$ with WENO-Z reconstruction are shown in Table.5. Here, the WENO-Z reconstruction for spatial derivatives is consistent with the HGKS when obtaining the high-fidelity DNS data [8].

References

- [1] Hussein Aluie. Compressible turbulence: the cascade and its locality. *Physical review letters*, 106(17):174502, 2011.
- [2] Alexei G Kritsuk, Rick Wagner, and Michael L Norman. Energy cascade and scaling in supersonic isothermal turbulence. *Journal of Fluid Mechanics*, 729, 2013.
- [3] Sanjiva K Lele. Compressibility effects on turbulence. *Annual review of fluid mechanics*, 26(1):211–254, 1994.
- [4] A Hanifi, PH Alfredsson, AV Johansson, and DS Hennigson. *Transition, Turbulence and Combustion Modelling: Lecture Notes from the 2nd ERCOFTAC Summerschool held in Stockholm, 10–16 June, 1998*, volume 6. Springer Science & Business Media, 2012.
- [5] Pierre Sagaut and Claude Cambon. *Homogeneous turbulence dynamics*, volume 10. Springer, 2008.
- [6] Eric Garnier, Nikolaus Adams, and Pierre Sagaut. *Large eddy simulation for compressible flows*. Springer Science & Business Media, 2009.
- [7] G Kumar, Sharath S Girimaji, and J Kerimo. Weno-enhanced gas-kinetic scheme for direct simulations of compressible transition and turbulence. *Journal of Computational Physics*, 234:499–523, 2013.
- [8] Guiyu Cao, Liang Pan, and Kun Xu. Three dimensional high-order gas-kinetic scheme for supersonic isotropic turbulence i: criterion for direct numerical simulation. *Computers & Fluids*, 192:104273, 2019.
- [9] Jianchun Wang, L-P Wang, Zuoli Xiao, Y Shi, and S Chen. A hybrid numerical simulation of isotropic compressible turbulence. *Journal of Computational Physics*, 229(13):5257–5279, 2010.
- [10] Jianchun Wang, Yipeng Shi, Lian-Ping Wang, Zuoli Xiao, XT He, and Shiyi Chen. Scaling and statistics in three-dimensional compressible turbulence. *Physical review letters*, 108(21):214505, 2012.
- [11] Ulrich Schumann. Subgrid scale model for finite difference simulations of turbulent flows in plane channels and annuli. *Journal of computational physics*, 18:376–404, 1975.
- [12] Akira Yoshizawa and Kiyosi Horiuti. A statistically-derived subgrid-scale kinetic energy model for the large-eddy simulation of turbulent flows. *Journal of the Physical Society of Japan*, 54(8):2834–2839, 1985.
- [13] Siniša Krajnović and Lars Davidson. A mixed one-equation subgrid model for large-eddy simulation. *International journal of heat and fluid flow*, 23(4):413–425, 2002.
- [14] Giuliano De Stefano, Oleg V Vasilyev, and Daniel E Goldstein. Localized dynamic kinetic-energy-based models for stochastic coherent adaptive large eddy simulation. *Physics of Fluids*, 20(4):045102, 2008.

- [15] Sutanu Sarkar, Gordon Erlebacher, M Yousuff Hussaini, and Heinz Otto Kreiss. The analysis and modelling of dilatational terms in compressible turbulence. *Journal of Fluid Mechanics*, 227:473–493, 1991.
- [16] Otto Zeman. On the decay of compressible isotropic turbulence. *Physics of Fluids A: Fluid Dynamics*, 3(5):951–955, 1991.
- [17] S Sarkar. The pressure–dilatation correlation in compressible flows. *Physics of Fluids A: Fluid Dynamics*, 4(12):2674–2682, 1992.
- [18] David C Wilcox. Dilatation-dissipation corrections for advanced turbulence models. *AIAA journal*, 30(11):2639–2646, 1992.
- [19] AM El Baz and BE Launder. Second-moment modelling of compressible mixing layers. In *Engineering Turbulence Modelling and Experiments*, pages 63–72. Elsevier, 1993.
- [20] JR Ristorcelli. A pseudo-sound constitutive relationship for the dilatational covariances in compressible turbulence. *Journal of Fluid Mechanics*, 347:37–70, 1997.
- [21] David C Wilcox et al. *Turbulence modeling for CFD*, volume 2. DCW industries La Canada, CA, 1998.
- [22] Akira Yoshizawa. Statistical theory for compressible turbulent shear flows, with the application to subgrid modeling. *The Physics of fluids*, 29(7):2152–2164, 1986.
- [23] Eric Pomraning and Christopher J Rutland. Dynamic one-equation nonviscosity large-eddy simulation model. *AIAA journal*, 40(4):689–701, 2002.
- [24] Noma Park and Krishnan Mahesh. Numerical and modeling issues in les of compressible turbulence on unstructured grids. In *45th AIAA Aerospace Sciences Meeting and Exhibit*, page 722, 2007.
- [25] Xiaochuan Chai and Krishnan Mahesh. Dynamic-equation model for large-eddy simulation of compressible flows. *Journal of Fluid Mechanics*, 699:385–413, 2012.
- [26] Jeffrey Slotnick, Abdollah Khodadoust, Juan Alonso, David Darmofal, William Gropp, Elizabeth Lurie, and Dimitri Mavriplis. Cfd vision 2030 study: a path to revolutionary computational aerosciences. 2014.
- [27] Joseph Smagorinsky. General circulation experiments with the primitive equations: I. the basic experiment. *Monthly weather review*, 91(3):99–164, 1963.
- [28] Massimo Germano, Ugo Piomelli, Parviz Moin, and William H Cabot. A dynamic subgrid-scale eddy viscosity model. *Physics of Fluids A: Fluid Dynamics*, 3(7):1760–1765, 1991.
- [29] Bert Vreman, Bernard Geurts, and Hans Kuerten. A priori tests of large eddy simulation of the compressible plane mixing layer. *Journal of engineering mathematics*, 29(4):299–327, 1995.
- [30] Albertus Willem Vreman. *Direct and large-eddy simulation of the compressible turbulent mixing layer*. Universiteit Twente, 1995.
- [31] M Pino Martin, Ugo Piomelli, and Graham V Candler. Subgrid-scale models for compressible large-eddy simulations. *Theoretical and Computational Fluid Dynamics*, 13(5):361–376, 2000.
- [32] Jianchun Wang, Minping Wan, Song Chen, and Shiyi Chen. Kinetic energy transfer in compressible isotropic turbulence. *Journal of Fluid Mechanics*, 841:581–613, 2018.
- [33] Prabhu Lal Bhatnagar, Eugene P Gross, and Max Krook. A model for collision processes in gases. i. small amplitude processes in charged and neutral one-component systems. *Physical review*, 94(3):511, 1954.
- [34] Sydney Chapman and TG Cowling. The mathematical theory of non-uniform gases: An account of the kinetic theory of viscosity, thermal conduction and diffusion in gases. cambridge mathematical library. *Cambridge University Press*, 1:27–52, 1970.
- [35] Kun Xu. A gas-kinetic bkg scheme for the navier–stokes equations and its connection with artificial dissipation and godunov method. *Journal of Computational Physics*, 171(1):289–335, 2001.
- [36] Kun Xu. *Direct modeling for computational fluid dynamics: construction and application of unified gas-kinetic schemes*. World Scientific, 2015.
- [37] Guiyu Cao, Hualin Liu, and Kun Xu. Physical modeling and numerical studies of three-dimensional non-equilibrium multi-temperature flows. *Physics of Fluids*, 30(12):126104, 2018.
- [38] Jiequan Li and Zhifang Du. A two-stage fourth order time-accurate discretization for lax–wendroff type flow solvers i. hyperbolic conservation laws. *SIAM Journal on Scientific Computing*, 38(5):A3046–A3069, 2016.

- [39] Liang Pan, Kun Xu, Qibing Li, and Jiequan Li. An efficient and accurate two-stage fourth-order gas-kinetic scheme for the euler and navier–stokes equations. *Journal of Computational Physics*, 326:197–221, 2016.
- [40] Liang Pan and Kun Xu. Two-stage fourth-order gas-kinetic scheme for three-dimensional euler and navier-stokes solutions. *International Journal of Computational Fluid Dynamics*, 32(10):395–411, 2018.
- [41] Xing Ji, Fengxiang Zhao, Wei Shyy, and Kun Xu. A family of high-order gas-kinetic schemes and its comparison with riemann solver based high-order methods. *Journal of Computational Physics*, 356:150–173, 2018.
- [42] Fengxiang Zhao, Xing Ji, Wei Shyy, and Kun Xu. Compact higher-order gas-kinetic schemes with spectral-like resolution for compressible flow simulations. *Advances in Aerodynamics*, 1(1):13, 2019.
- [43] Shuang Tan, Qibing Li, Zhixiang Xiao, and Song Fu. Gas kinetic scheme for turbulence simulation. *Aerospace Science and Technology*, 78:214–227, 2018.
- [44] Guiyu Cao, Hongmin Su, Jinxiu Xu, and Kun Xu. Implicit high-order gas kinetic scheme for turbulence simulation. *Aerospace Science and Technology*, 92:958–971, 2019.
- [45] Ravi Samtaney, Dale I Pullin, and Branko Kosović. Direct numerical simulation of decaying compressible turbulence and shocklet statistics. *Physics of Fluids*, 13(5):1415–1430, 2001.
- [46] Thierry Passot and Annick Pouquet. Numerical simulation of compressible homogeneous flows in the turbulent regime. *Journal of Fluid Mechanics*, 181:441–466, 1987.
- [47] Stephen B Pope. Turbulent flows, 2001.
- [48] Vinayak Eswaran and Stephen B Pope. An examination of forcing in direct numerical simulations of turbulence. *Computers & Fluids*, 16(3):257–278, 1988.
- [49] Ugo Piomelli, William H Cabot, Parviz Moin, and Sangsan Lee. Subgrid-scale backscatter in turbulent and transitional flows. *Physics of Fluids A: Fluid Dynamics*, 3(7):1766–1771, 1991.
- [50] Bert Vreman, Bernard Geurts, and Hans Kuerten. Realizability conditions for the turbulent stress tensor in large-eddy simulation. *Journal of Fluid Mechanics*, 278:351–362, 1994.
- [51] Alexandre Favre. Equations des gaz turbulents compressibles. *J. de Mecanique*, 4(3), 1965.
- [52] Leslie SG Kovaszny. Turbulence in supersonic flow. *Journal of the Aeronautical Sciences*, 20(10):657–674, 1953.
- [53] Marcos Castro, Bruno Costa, and Wai Sun Don. High order weighted essentially non-oscillatory weno-z schemes for hyperbolic conservation laws. *Journal of Computational Physics*, 230(5):1766–1792, 2011.
- [54] Parviz Moin, Kyle Squires, W Cabot, and Sangsan Lee. A dynamic subgrid-scale model for compressible turbulence and scalar transport. *Physics of Fluids A: Fluid Dynamics*, 3(11):2746–2757, 1991.
- [55] Solomon Kullback and Richard A Leibler. On information and sufficiency. *The annals of mathematical statistics*, 22(1):79–86, 1951.